Earthquakes and Structures, *Vol. 17, No. 2 (2019) 233-244*
DOI: https://doi.org/10.12989/eas.2019.17.2.233

Anti-seismic behavior of composite precast utility tunnels based on pseudo-static tests

Yanmin Yang[1], Xinru Tian[*1], Quanhai Liu[2], Jiabo Zhi[2] and Bo Wang[1]

[1] *School of Civil Engineering, Jilin Jianzhu University, Changchun 130118, China*
[2] *Jilin Senhuang Building Materials Group Co., Ltd., Jilin 130200, China*

(Received February 1, 2019, Revised May 23, 2019, Accepted June 6, 2019)

Abstract. In this work, we have studied the effects of different soil thicknesses, haunch heights, reinforcement forms and construction technologies on the seismic performance of a composite precast fabricated utility tunnel by pseudo-static tests. Five concrete specimens were designed and fabricated for low-cycle reciprocating load tests. The hysteretic behavior of composite precast fabricated utility tunnel under simulated seismic waves and the strain law of steel bars were analyzed. Test results showed that composite precast fabricated utility tunnel met the requirements of current codes and had good anti-seismic performance. The use of a closed integral arrangement of steel bars inside utility tunnel structure as well as diagonal reinforcement bars at its haunches improved the integrity of the whole structure and increased the bearing capacity of the structure by about 1.5%. Increasing the thickness of covering soil within a certain range was beneficial to the earthquake resistance of the structure, and the energy consumption was increased by 10%. Increasing haunch height within a certain range increased the bearing capacity of the structure by up to about 19% and energy consumption by up to 30%. The specimen with the lowest haunch height showed strong structural deformation with ductility coefficient of 4.93. It was found that the interfaces of haunches, post-casting self-compacting concrete, and prefabricated parts were the weak points of utility tunnel structures. Combining the failure phenomena of test structures with their related codes, we proposed improvement measures for construction technology, which could provide a reference for the construction and design of practical projects.

Keywords: composite precast fabricated utility tunnel; anti-seismic performance; failure modes; steel strain analysis; technique improvement

1. Introduction

As an important part of urban infrastructure, underground structure plays an irreplaceable role. However, in the face of earthquake force majeure, shallow-buried rectangular structures, such as box culverts and rectangular tunnels, will be affected by vibration damage.

Several researchers around the world have done research in this field and accumulated some achievements. Based on the shear deformation capacity, Nishioka and Unjoh (2003) presented a simplified evaluation method for seismic performance of underground public facilities with rectangular cross-section. Through large shaking table test and correlation analysis, Matsui *et al*. (2004) established and verified a nonlinear FEM model suitable for seismic behavior of underground structures, and strengthened the skeleton and hysteresis rules for RC members. By means of a series of shaking table tests and numerical analysis, Jiang *et al.* (2010) studied the performance of a scaled utility tunnel model under earthquake excitation. Through a series of shaking table tests, Chen *et al.* (2010) have studied the performance of utility tunnel with or without construction joints under the excitation of non-uniform seismic waves. Debiasi *et al.* (2013) have studied the scope and limitation of the simplified calculation methods for shallow-buried rectangular structures which used to estimate its seismic response. Abuhajar *et al*. (2015) studied the static response of box culvert constructed by embankment installation method through a series of centrifuge tests and numerical model using FLAC 2D. Ulgen *et al*. (2015) carried out a series of dynamic centrifugal tests on a box-shaped flexible underground structure under the harmonic motions of different accelerations and frequencies to analyze its dynamic characteristics. Huang *et al*. (2016) used matrix force method to analyze the deformation of underground box structure in elastic half space. Based on the analysis of inelastic frame, Park *et al*. (2016) studied the collapse mechanism of rectangular cut-and-cover tunnels under seismic loading. Ertugrul (2016) studied the dynamic behavior and lateral earth pressures of box culverts buried in dry cohesionless soils by numerical simulation. Zou *et al*. (2017) proposed an improved Finite Element method called New Pseudo-Static Analysis (NewPSA) to predict the nonlinear behavior of underground frame structures subjected to increasing horizontal seismic excitations. Tsinidis (2017) studied the numerical parameterization of the transversal seismic response of rectangular tunnels buried in soft soil. Ma *et al.* (2018) studied the seismic behavior of underground rectangular structures under different buried depths by numerical analysis. Xu *et al.* (2018) combined with practical engineering, studied the

∗Corresponding author, Postgraduate Student
E-mail: 962364282@qq.com

ISSN: 2092-7614 (Print), 2092-7622 (Online)

(a) Steel cage after lashing (b) Molding (c) Pasting strain gauges

(d) Pouring concrete (e) Prefabricated panels (f) Assembling

Fig. 1 Construction of composite precast fabricated utility tunnels

influence of many key factors on seismic response, such as seismic load conditions, structural inertia effect, relative stiffness of soil-structure, soil-structure interface characteristics and so on. Nguyen *et al.* (2019) established the seismic fragility curves of rectangular cut-and-cover tunnels based on the analysis of non-linear frame. Ma *et al.* (2019) carried out a detailed numerical study on seismic response of underground rectangular structures, and discussed the role of structural members before and during earthquakes.

Underground utility tunnels integrate various engineering equipment such as electricity, communication, gas, heat supply, water, drainage, etc. They are an important infrastructure and serve as a 'lifeline' for urban operations. When an earthquake strikes, underground utility tunnels can be damaged to varying degrees, and in severe cases, the entire city can malfunction. Therefore, it is of great significance to study the seismic performance of underground utility tunnels.

Due to vigorous promotion of prefabricated building structures in China, the development of a convenient, efficient and low-cost assembly and stacking technique for pipe racks is of significant practical importance. In this study, seismic tests were conducted on composite precast fabricated utility tunnels independently developed by Jilin Senhuang Building Materials Group Co., Ltd. Based on different soil thicknesses, haunch heights, reinforcement forms and construction technologies, five utility tunnel specimens were designed and fabricated for low cycle reciprocating load tests. We also comprehensively evaluated the seismic performances of these composite precast fabricated utility tunnels and proposed process improvement measures based on current codes and test failure characteristics, which could provide a reference for the application of these composite precast fabricated utility tunnels in practical projects.

2. Test background

2.1 Construction process of composite precast fabricated utility tunnels

To construct a utility tunnel, first its top, bottom, and wall plates were prefabricated, and then assembled into a monolithic structure by self-compacting concrete. Construction process is shown in Fig. 1. The longitudinal reinforcement of each haunch on the board had a certain anchor length to be able to effectively connect adjacent boards. A level gauge was used to ensure that the two prefabricated panels were vertically aligned. Once the two plates were connected, diagonal supports were connected to utility tunnel by means of pre-embedded bolts to ensure the overall stability of the structure and facilitate the post-casting of self-compacting concrete. After tying the steel bars, the other plates except the top plate were poured with 57 mm thick concrete on one side. After curing for a period of time, the other side was poured with 51 mm thick concrete, and the top plate was only poured on one side, and the concrete thickness was 51 mm. After the prefabricated panels have reached the design strength, they are assembled. After the self-compacting concrete is poured, the template of the corner and the section position is removed for 2-3 days, and the natural state is cured for 30 days, and the shape is cured.

2.2 Design of the test utility tunnels

According to construction process developed by the company, five composite precast fabricated utility tunnels were designed and fabricated (PG1 to PG5) with dimensions of 1500×1500×1000 (mm^3), cover concrete thickness of 34 mm, and wall thickness of 200 mm, as shown in Fig. 2. The compressive strength of test utility tunnels was 40 MPa at 28 days age. Design and reinforcement parameters are shown in Tables 1-2.

Truss steel bars were arranged centrally 800 mm from the top plates, 900 mm from the wall plates and 1000 mm from the bottom plates of each specimen. The oblique

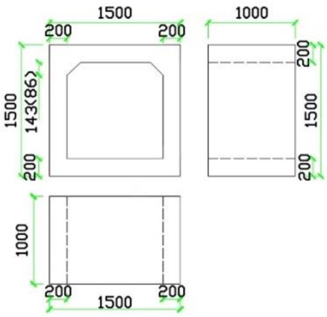

Fig. 2 Dimensional drawing of the utility tunnel

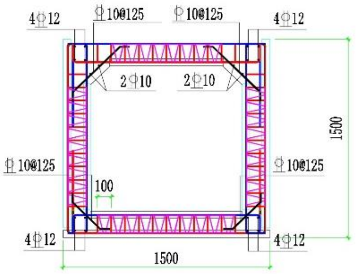

Fig. 3 PG2, PG3 (with diagonal reinforcement at the bottom)

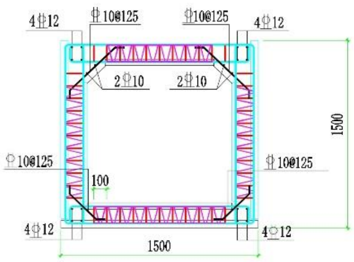

Fig. 4 PG4 (closed monolithic)

reinforcement of the bottom haunch of PG5 was Φ10@100 in the thickness direction. The reinforcements of utility tunnels are shown in Figs. 3-6. The data in parentheses in Fig. 5 is where PG5 differs from PG1, PG2, and PG3.

2.3 Test design

2.3.1 Loading devices

Loading devices included horizontal, vertical, restraining and connecting devices. In order to simulate the actual working stresses of utility tunnels and meet test requirements, vertical loading had to be consisted of two parts. Multi-point loading equivalent replaced uniform load using a distribution beam, and pre-stress was applied at the intersection of ceiling and walls. The two parts cooperated to simulate the thickness of the upper cover soil and limit vertical displacement to prevent the uplift of utility tunnel structures during the test. Quasi-static test method and US MTS hydraulic servo control system were used to apply horizontal low-cycle reciprocating load to the center of top plates. Joints and steel tie rods were designed based on the size and ultimate bearing capacity of specimens. Bottom limit steel beam was designed in such a way to be consistent with the thickness of bottom plate. Test loading devices are shown in Fig. 7.

Table 1 Design parameters of utility tunnels

Number of specimen	Cover earth thickness (m)	Reinforcement form (with or without diagonal reinforcement at the bottom)	Construction process	Top haunch height (mm)
PG1	2.5	Without	Segmented binding	143
PG2	2.5	With	Segmented binding	143
PG3	5	With	Segmented binding	143
PG4	2.5	With	Closed monolithic	143
PG5	2.5	With	Segmented binding	86

2.3.2 Loading system

Under 65 and 130 kN vertical loads, the thickness of the covering soil in simulation was considered to be 2.5 and 5.0 m, respectively. The horizontal seismic force in the simulation was applied by displacement control method. In order to eliminate the effect of strain rate on test results, initial displacement increment was adjusted at 1 mm. When the displacement reached 4 mm, the displacement increment was expanded to 2 mm and each stage was cycled twice. Test was terminated when the bearing capacity of test specimen dropped to 85% of the ultimate load or load could not be continued.

2.3.3 Monitoring plan

MTS actuator was connected to UK IMP data acquisition system for simultaneous acquisition and automatic generation of load-displacement hysteresis diagrams, steel strains, utility tunnel displacements and tunnel crack development. IMP data acquisition system is shown in Fig. 8.

3. Test failure phenomenon and damage mechanism analyses

Table 2 Reinforcement parameters of utility tunnels

Panels (top, bottom and wall panels)				Haunches		
Reinforcing mesh		Truss bars		Long steel bars (The thickness direction)	Diagonal reinforcement	Upper diagonal reinforcement
Main bearing reinforcement	Reinforcement perpendicular to the main reinforcement	Chord member	Web member			
Φ12@125	Φ10@100	3Φ8	Φ6	4Φ12	Φ10@125	2Φ10

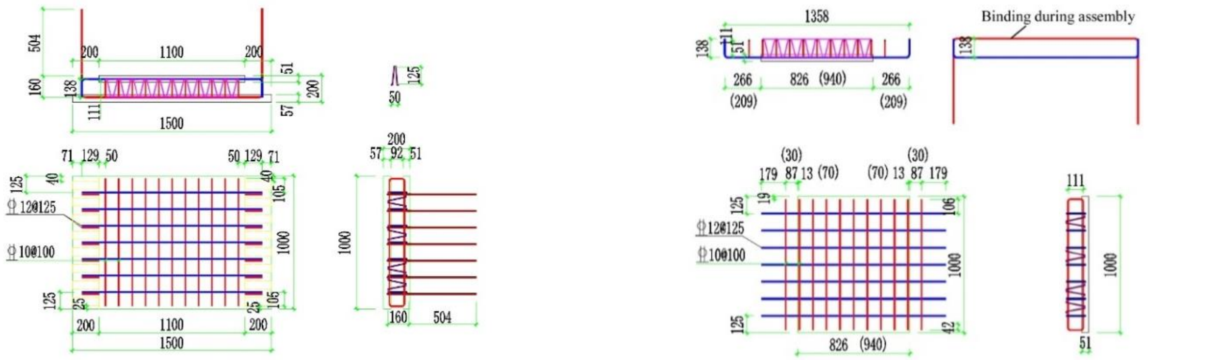

(a) Reinforcement in bottom plates of PG1, PG2, PG3, PG5 (b) Reinforcement in top plates of PG1, PG2, PG3, PG5

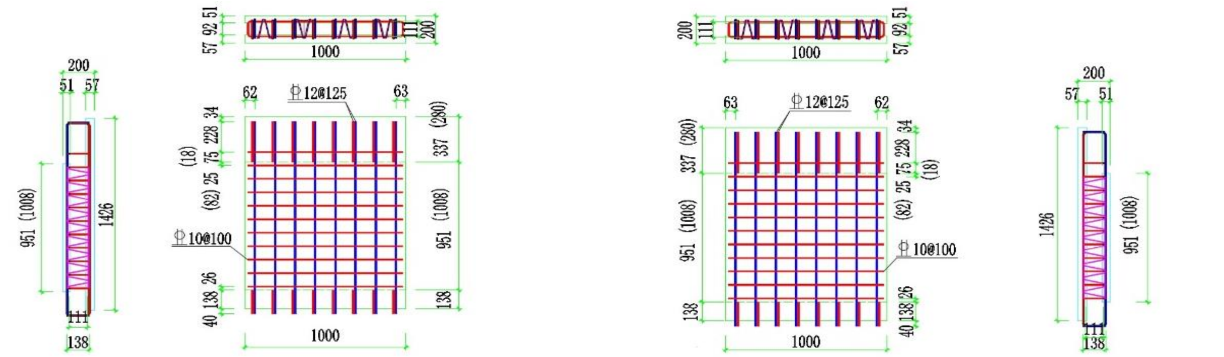

(c) Reinforcement in left panels of PG1, PG2, PG3, PG5 (d) Reinforcement in right panels of PG1, PG2, PG3, PG5

Fig. 5 Reinforcement diagrams of each plate in PG1, PG2, PG3 and PG5 (segment lashing)

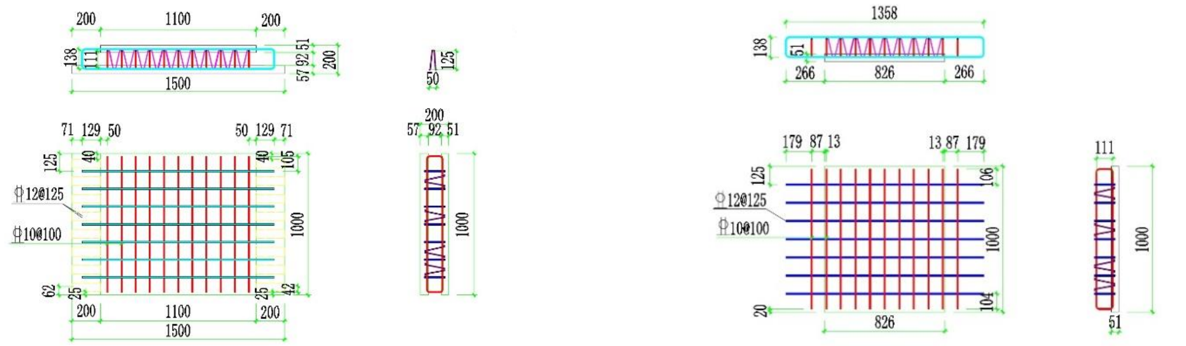

(a) Reinforcement in bottom plates of PG4 (b) Reinforcement in top plates of PG4

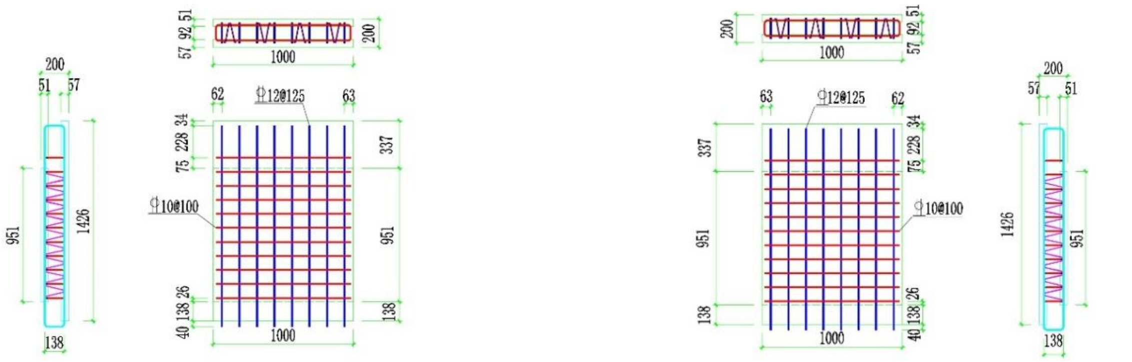

(c) Reinforcement in left panels of PG4 (d) Reinforcement in right panels of PG4

Fig. 6 Reinforcement diagrams of each plate in PG4 (closed monolithic)

3.1 Test failure phenomena of composite precast fabricated utility tunnels

The damage phenomena of the five test specimens are shown in Fig. 9. Each specimen was subjected to bending

Fig. 7 Test device setup

Fig. 8 IMP data acquisition system

failure. Failure processes and modes were similar in all specimens. Here, PG2 destruction process is described as an example. At the displacement angle of 1/500, the test piece was in elastic stage and no cracks occurred. However, at the displacement angle of 1/150, diagonal cracks occurred at top haunches. When displacement angle reached 1/125, the side of wall panel was cracked in horizontal direction. At the displacement angle of 1/83, oblique cracks occurred at top haunches and continued to develop and extend, and vertical cracks appeared due to the shearing of top plate near haunches. At the displacement angle of 1/57, the interface of post-casting self-compacting concrete and prefabricated part was cracked. When the displacement angle reached 1/46, a number of new cracks appeared at top plate near haunches, top haunches, and above wall panel. At

(a) Front utility tunnel Section in the direction of observation (b) Rear utility tunnel section in the direction of observation (c) Left wall panel in the direction of observation (d) Right wall panel in the direction of observation

Test failure phenomenon of PG1

(a) Front utility tunnel section in the direction of observation (b) Rear utility tunnel section in the direction of observation (c) Left wall panel in the direction of observation (d) Right wall panel in the direction of observation

Test failure phenomenon of PG2

(a) Front utility tunnel section in the direction of observation (b) Rear utility tunnel section in the direction of observation (c) Left wall panel in the direction of observation (d) Right wall panel in the direction of observation

Test failure phenomenon of PG3

Fig. 9 Test failure phenomena of composite precast fabricated utility tunnels

(a) Front utility tunnel section in the direction of observation

(b) Rear utility tunnel section in the direction of observation

(c) Left wall panel in the direction of observation

(d) Right wall panel in the direction of observation

Test failure phenomenon of PG4

(a) Front utility tunnel section in the direction of observation

(b) Rear utility tunnel section in the direction of observation

(c) Left wall panel in the direction of observation

(d) Right wall panel in the direction of observation

Test failure phenomenon of PG5

Fig. 9 Continued

the displacement angle of 1/31, vertical cracks of the interface of post-casting compacted concrete and prefabricated part penetrated the entire section of the hole. A large number of transverse cracks appeared at haunches, wall panels and roof panels, while surface cracks developed smoothly. Finally, at the displacement angle of 1/23, no new cracks appeared on the surface of the specimen, and PG2 reached its ultimate bearing capacity and experienced bending failure.

As can be seen in Fig. 9, the destruction of composite precast fabricated utility tunnels mainly occurred at haunches, especially bottom haunches, which were the weakest parts of the structures. In later stages of loading, specimens entered plastic stage. The interfaces of post-cast self-compacting concrete and prefabricated member were delaminated, and overall mechanical performance was affected. The directions of cracks in the walls of all specimens were horizontal and concentrated in the middle and upper sections of the walls. Wall panels were damaged by bending. In PG2 wallboard, upper horizontal cracks were dense and several horizontal cracks appeared in lower part. In PG1 wallboard, upper horizontal cracks were small and the distances between cracks were large, indicating that diagonal reinforcing bars at bottom haunches enhanced structural integrity and improved force transmission in the structure. The number of horizontal cracks in PG3 wallboard was fewer than that of PG2 and the distances between cracks in PG3 were larger. This was because higher thicknesses of covering soil increased the constraint of utility tunnel and inhibited crack generation. The development trend of horizontal cracks in PG4 and PG2 wallboards was similar. However, failure displacement of PG4 was 17.9% higher than that of PG2. This indicated that the deformation of utility tunnel structures with closed monolithic reinforcements was stronger. After decreasing haunch heights in PG5 wallboard, upper horizontal cracks became smaller than those in PG2 and the distances between cracks were larger. Structural bearing capacity and energy consumption of PG5 were decreased by 15.7% and 23.4%, respectively, but its structural deformation ability was higher.

3.2 Analysis of damage mechanism

In practical applications, the utility tunnel is buried underground, and its left and right wall panels have earth pressure, which is beneficial to the utility tunnel under horizontal seismic loads, and can provide lateral force to suppress lateral displacement or deformation. The test considers that if there is better seismic performance without the lateral soil's favorable effect on the utility tunnel, the application is more reliable in practice. As can be seen in Fig. 9, since the interface of wall panel and bottom plate was subjected to self-weight and horizontal shearing force of utility tunnel and overlying soil, it was subjected to higher stress. Concrete at the bottom haunches of utility tunnel was more seriously damaged than those at top haunches, and covering concrete layer was sometimes peeled off. The most severe tensile damages occurred at bottom plates and its haunches while the most severe pressure damages occurred at top plates and its haunches. In the experimental design of this paper, diagonal reinforcements were added to corner *L*-shaped joint areas to disperse the tensile stress of concrete, and haunches

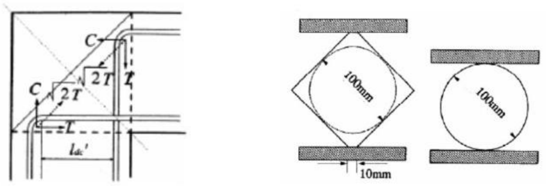

(a) Calculation model of cracking force (b) Equivalent analysis of splitting in joint zone

Fig. 10 Analysis of cracking force in *L*-shaped joint zones

increased resistance moment which enhanced node performance. However, many oblique cracks occurred at the top corners of utility tunnel. This was due to repeated push-pull actions of the same curvature, which caused the joint zone to crack along the twisting direction, and more cracks were generated along the principal compressive stress line.

Assuming that concrete pressure (*C*) and steel tensile force (*T*) were equal, the force analysis of joint zones was simplified to cylindrical splitting force. The force analysis is shown in Fig. 10. The cracking force was calculated as Eq. (1) (Kong 2014).

$$\sqrt{2}T = \frac{\pi \cdot l'_{dc} \cdot b \cdot \kappa f_{sp}}{2} \tag{1}$$

where l'_{dc} is the length of *L*-shaped corner joint (the distance from the inner edge of the steel bar to the inner edge of the longitudinal anchor); *b* is the longitudinal length of node area; κ is the conversion factor of the tensile strength of cube; the tensile strength of cylinder is usually assumed to be 1.2. f_{sp} is the tensile crack strength of cube.

4. Test results analysis

4.1 Hysteresis curve analysis

The hysteresis curves of each specimen under different variables are shown in Fig. 11.

The following conclusions were drawn based on Fig. 11:

(1) At initial loading stage, the specimen was in elastic stage and the curve was basically linear. As displacement was increased, the area of hysteresis loop was also increased. However, as cracks continued to develop and the cumulative damage of specimen was increased, the stiffness of the structure was gradually decreased and there was a large residual deformation during unloading. Pinching phenomenon was obvious in later hysteresis curves (inversed *S* shape), and the structure still showed good energy consumption.

(2) As can be seen in Fig. 11(a), the hysteresis curve of PG2 was larger than that of PG1, and this was more obvious during reverse loading. This phenomenon indicated that arranging diagonal reinforcements at bottom haunches improved the integrity and seismic performance of entire structure.

(3) As can be seen in Fig. 11(b), the hysteresis loop area of PG3 at the initial stage of loading was smaller than that of PG2. By the increase of displacement, the hysteresis loop area of PG3 grew larger than that of PG2, and the bearing capacity of PG3 decreased significantly when utility tunnel reached its ultimate bearing capacity. This phenomenon revealed that soil thickness had a great effect on the seismic performance of utility tunnel.

(4) It can be seen in Fig. 11(c) that the hysteresis curve of PG4 was the largest among all test specimens with different variables, indicating that the seismic performance of composite precast fabricated utility tunnels with closed monolithic reinforcement was higher than those with segmented lashing reinforcement.

(5) It can be seen in Fig. 11(d) that the bearing capacity of utility tunnel was significantly improved by increasing haunch heights.

4.2 Energy consumption analysis

Energy consumption capacity refers to the envelope

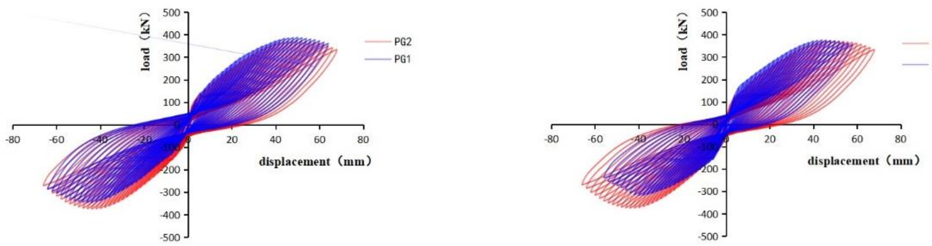

(a) Different reinforcement forms (b) Different soil thickness

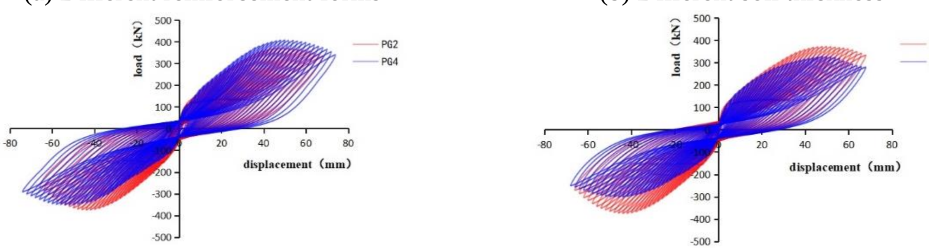

(c) Different construction processes (d) Different corner heights

Fig. 11 Hysteresis curves

Table 3 Calculation results of energy consumption

Variables	Number of Specimen		Energy consumption under load displacement (kN.mm)					
			10 mm	20 mm	30 mm	40 mm	50 mm	60 mm
Reinforcement form (with or without diagonal reinforcement at the bottom)	PG1	Without	810	1693	2340	3755	6650	10010
	PG2	With	1032	1734	2698	4396	7376	10678
	The effect of arranging diagonal reinforcement on energy consumption		27.4% (↑)	2.4% (↑)	15.3% (↑)	17.1% (↑)	10.9% (↑)	6.7% (↑)
Covering soil thickness (m)	PG2	2.5	1032	1734	2698	4396	7376	10678
	PG3	5	886	1694	2759	4521	8124	-
	Effect of increasing soil thickness on energy consumption		21.5% (↓)	2.3% (↓)	2.3% (↑)	2.8% (↑)	10.1% (↑)	-
Construction process	PG2	Segmented binding	1032	1734	2698	4396	7376	10678
	PG4	Closed monolithic	976	1855	2816	4616	7546	11052
	Effect of closed monolithic steel bars on energy consumption		5.4% (↓)	6.9% (↑)	4.4% (↑)	5.0% (↑)	2.3% (↑)	3.5% (↑)
Height of the top haunch (mm)	PG5	86	790	1721	2530	4108	7091	9326
	PG2	143	1032	1734	2698	4396	7376	10678
	The effect of large haunch height on energy consumption		30.6% (↑)	0.8% (↑)	6.6% (↑)	7.0% (↑)	4.0% (↑)	14.5% (↑)

Table 4 Characteristic values of test control

Number of specimen	Loading direction	Crack load		Yield load		Peak load		Ultimate load		Ductility factor
		P_{cr} / kN	Δ_{cr} / mm	P_y / kN	Δ_y / mm	P_p / kN	Δ_p / mm	P_u / kN	Δ_u /mm	$\mu=\Delta_u/\Delta_y$
PG1	Forward direction	112	3.8	266	19.7	387	50	361	64	3.25
	Negative direction	70	3.7	227	20	347	46	297	62	3.10
	Mean	91	3.75	246.50	19.85	367	48	329	63	3.17
PG2	Forward direction	116	3.9	237	17.9	372	49.8	341	65.7	3.67
	Negative direction	116	3.9	234	15.9	375	43.8	317	59.8	3.76
	Mean	116	3.9	258	16.90	373.50	46.80	329	62.75	3.71
PG3	Forward direction	128	3.8	271	19.7	376	44	356	58	2.94
	Negative direction	123	3.7	216	13.8	318	39.7	268	52	3.77
	Mean	125.50	3.75	243.50	16.75	347	41.85	312	55	3.28
PG4	Forward direction	124	5.4	245	17.8	407	52	340	74	4.16
	Negative direction	118	5.8	200	18	351	54	292	74	4.11
	Mean	121	5.60	222.50	17.90	379	53	316	74	4.13
PG5	Forward direction	112	3.8	207	13.8	328	50	280	68	4.93
	Negative direction	104	3.7	180	13.8	302	46	252	68	4.93
	Mean	108	3.75	193.50	13.8	315	48	266	68	4.93

areas of hysteresis curves under different loadings, reflecting the comprehensive process of energy absorption and dissipation in the component. Calculation results are summarized in Table 3.

The following conclusions were drawn based on the data summarized in Table 3.

(1) The energy consumption of each specimen was increased by increasing displacement. All five utility tunnels showed good energy consumptions.

(2) The application diagonal reinforcements at bottom haunches improved the energy consumption of utility tunnel. In this case, when loading displacement was in the range of 0-10 mm, the energy consumption of utility tunnel was increased by 27.4%. When loading displacement was increased to 20-40 mm, the energy consumption of utility tunnel kept increasing. During the loading of specimen, obvious cracks occurred at the surface of specimen, damage degree increased, and energy consumption was decreased.

(3) After increasing soil thickness, crack development during pre-loading was inhibited, and structural energy consumption was decreased. But this improved the energy consumption capacity of utility tunnel in later loading stages. At the end of loading, the energy consumption of utility tunnel was increased by up to 10.1%.

(4) The energy consumption of utility tunnel using closed monolithic reinforcement was increased by up to 6.9% compared to that using segmented lashing reinforcement.

(5) Within a certain range of haunch heights, higher haunch heights provided greater energy consumptions in utility tunnel. Compared with the small haunch height, the energy consumption of utility tunnel with higher haunch height increased up to 30.6%, and seismic performance was good.

4.3 Skeleton curve analysis

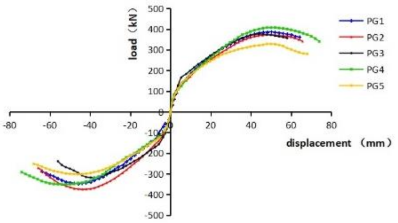

Fig. 12 Skeleton curves

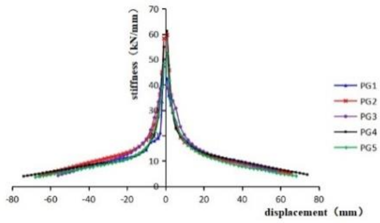

Fig. 13 Stiffness degradation curves

Skeleton curve is the envelope connecting the extreme points of the hysteresis loop of each stage. The skeleton curves of different specimens are shown in Fig. 12. Test control characteristic values are shown in Table 4.

The following conclusions were drawn from Fig. 12 and Table 4.

(1) The cracking and peak displacement of PG2 were similar to those of PG1; however, the cracking and peak loads of PG2 were higher than those of PG1, and the ductility coefficient of PG2 was 17.03% higher than that of PG1. These indicated that the arrangement of diagonal reinforcement at bottom corners increased the cracking load and ultimate bearing capacity of utility tunnel. PG2 had good overall force performance and better deformation ability under reciprocating load.

(2) Cracking, yielding, peaking and failure displacement of PG3 were lower than those of PG2, and its ductility coefficient was 11.59% lower than that of PG2. This verified that utility tunnel was strengthened by the restraining soil after increasing soil thickness.

(3) Cracking, yielding, peaking and failure displacement of PG4 were higher than those of PG2, and its ductility coefficient was 11.32% higher than that of PG2. This showed that the overall performance of utility tunnels with closed monolithic reinforcement was high, which suppressed the cracking, yielding and damage of test structure, and also improved ductility and structural earthquake resistance.

(4) The ductility coefficient of PG5 was 4.93, but its yield displacement was the smallest among all specimens, indicating that lower haunch heights improved the ductility of utility tunnel, but it did not delay the yielding stage of structures.

4.4 Analysis of stiffness degradation curve

Stiffness degradation curves reflect the cumulative damage of the structure, which is an important part of the analysis of the seismic performance of structure. Stiffness degradation curves of each test specimen are shown in Fig. 13.

The following conclusions were drawn from Fig. 13.

(1) At initial loading stage, the specimen was stiff and its stiffness was attenuated very quickly by loading. After the specimen was yielded, with the increase of loading displacement, the cracks of utility tunnel the cumulative damage increased, which resulted in the decrease of the stiffness degradation rate of the specimens. When the specimen reaches their energy dissipation limit, stiffness degradation tended to be stable.

(2) The initial stiffness of PG2 was 31% higher than that of PG1, and its ultimate stiffness was 7.8% lower than that of PG1. This indicated that the application of diagonal reinforcements at bottom haunches significantly improved the rigidity of utility tunnel and effectively inhibited stiffness degradation.

(3) The rate of stiffness degradation of PG2 was higher than that of PG3 before the specimen was yielded. After the specimen was yielded, the stiffness degradation curve of PG2 was flatter than that of PG3. The stiffness degradation of the initial test structure was due to the cracking of concrete, and the increase of soil thickness suppressed crack development. In later loading stages, increasing covering soil thickness accelerated the stiffness degradation of the specimen.

(4) The stiffness values and trends of PG2 and PG4 were similar. However, the failure displacement of PG4 was larger than that of PG2, which indicated that the structural deformation ability of utility tunnels with closed monolithic reinforcements was stronger, but reinforcement method had little effect on the stiffness of the structure.

(5) The initial and ultimate stiffness values of PG2 were 15.7% and 20.5% higher than those of PG5, respectively. This revealed that higher haunch heights increased the rigidity of utility tunnel, and higher corners could delayed rigidity degradation of the structure.

5. Strain analysis of steel bars

By observing the damage of specimens, it was found that steel bars at haunches were seriously damaged, and diagonal reinforcing bars strengthened the joints. Therefore, steel bar test points at haunches were selected to analyze the displacement-strain relationship of steel bars under simulated seismic forces. The arrangement of steel strain measurement points are shown in Fig. 14. There is no diagonal reinforcing bar at the bottom of the PG1 test piece, and the position of the upper corner steel bar measuring points X1 and X2 is the same as other test pieces.

Tensile tests were performed on diagonal reinforcements at haunches, and yield strength f_{yk} was obtained to be 404.24 MPa, ultimate strength f_{stk} was found to be 553.68 MPa, and elastic modulus ES was determined to be 209.65 GPa. Yield and ultimate strains were 1928.166 and 2640.97 με, respectively. Strain analysis was performed on diagonal reinforcing bars at the haunches of each test structure (upper haunch steel angle measuring points X1 and X2, and lower haunch steel bar measuring points X3 and X4). Displacement-strain relationship diagram is shown in Fig. 15.

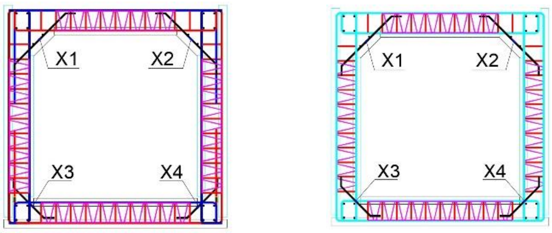

(a) PG2, PG3, PG5 (b) PG4

Fig. 14 Arrangement of steel test points

The following conclusions were drawn from Fig. 15.

(1) Under repeated loadings, the strain values of diagonal reinforcements at the haunches of utility tunnels were basically positive, indicating that diagonal reinforcements of haunches were subjected to tensile stress.

(2) Fig. 15(a) shows that test points X1 and X2 of PG1 and PG2 on diagonal reinforcements had reached yielding strains. The displacement-strain diagrams of test points X1 and X2 of PG2 were basically symmetrical, while the displacement-strain diagrams of steel points X1 and X2 of PG1 abruptly changed during later stages. This indicated that the arrangement of diagonal reinforcing bars at haunches strengthened the joints and enhanced the integrity of test structures; therefore, structural stress performance was better.

(3) It can be seen in Fig. 15(b) that the oblique reinforcing steel test points X1 and X2 of PG3 had not reached yield strain. This was because the increase of covering soil thickness inhibited crack generation in the early stages of loading, but crack development was intensified in later stages. The utilization rate of steel bar was low during the whole loading process.

(4) Fig. 15(c) shows that the strain values of oblique reinforcing bars X3 and X4 at the lower haunches of PG2 and PG4 were basically symmetrical with respect to loading direction, and both reached yield strain. The X3 test point of PG4 reached its ultimate strain and then broke.

(5) Fig. 15(d) shows that strain at X1 and X2 test points of PG5 gradually increased and yielded under repeated loadings. This indicated that decreasing haunch heights had greater effect on the mechanical mechanism of diagonal reinforcements, and significantly improved structural deformation ability.

6. Process improvement measures for composite precast fabricated utility tunnels

The failure of composite precast fabricated utility tunnels mainly occurs at haunches and interfaces of post-casting self-compacting concrete and prefabricated members. Combining damage phenomenon and experimental results, we proposed the following improvement measures for construction process, which could provide a reference for practical engineering applications.

(1) The damaging phenomena of each haunch of PG5 are shown in Fig. 16. In line with current codes (China General Institute of Nonferrous Engineering Design and Reasearch 2003), the measures shown in Fig. 17 were proposed. The length of the longitudinal reinforcement of overhanging floor was increased, and floor haunches were strengthened. These measures were convenient for construction and decreased the stress concentration of the structure.

(2) Under the action of earthquake, the top plate of utility tunnel was weakly stressed, and the bottom plate was stressed more seriously. The connection parts between side plates and bottom plate were the most damaged parts, and the seismic resistances of these parts had to be strengthened. To decease the effect of the delamination of the interfaces of post-casting self-compacting concrete and prefabricated parts, the original two interfaces were replaces with one interface. In other words, only one side of the bottom plate

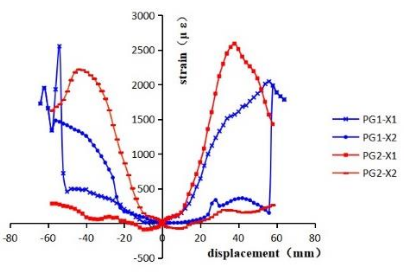

(a) Different reinforcement forms (X1, X2 measurement points)

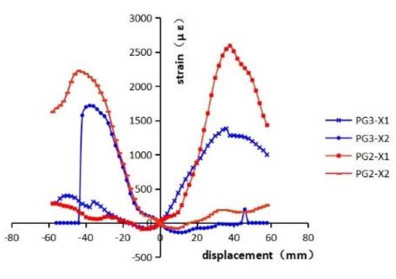

(b) Different soil thicknesses (X1, X2 measuring points)

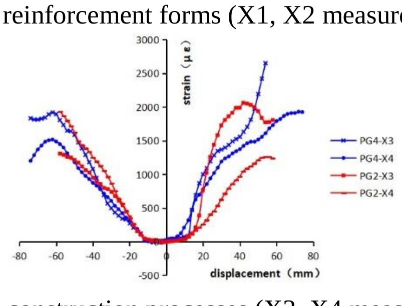

(c) Different construction processes (X3, X4 measuring points)

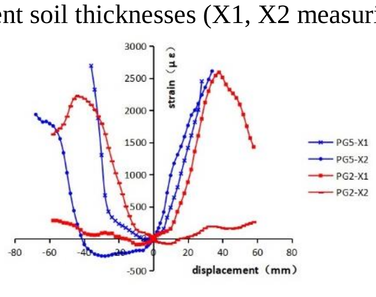

(d) different haunch heights (X1, X2 measuring points)

Fig. 15 Displacement-strain relationship diagrams of oblique reinforcement at haunches

Fig. 16 Destruction of upper and lower haunches

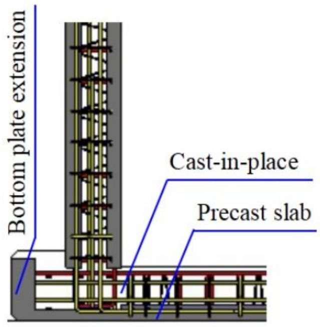

Fig. 17 Process improvement method at bottom haunches

was prefabricated and its other side was cast-in-place, which accelerated construction speed and ensured the integrity of utility tunnel.

7. Conclusions

- In this study, composite precast fabricated utility tunnels were subjected to bending failure. Cracks were mainly distributed at the haunches of utility tunnels, the interfaces of post-casting self-compacting concrete and prefabricated parts, and the middle and upper parts of wallboards. According to current codes and damage phenomena, the following improvement measures were proposed for utility tunnel construction process: increasing the length of steel bars at both ends of bottom plates to strengthen bottom haunches and constructing bottom plates by two pouring methods.
- The arrangement of diagonal reinforcements at bottom haunches of the assembled superimposed utility tunnel improved the ultimate bearing capacity of test utility tunnels and enhanced the integrity and structural deformation ability of test structures. In this case, the ductility coefficient of structure was increased by 17.03%.
- Increasing covering soil thickness within a certain range increased the energy consumption capacity of utility tunnel during later stages of loading. In this way, the energy consumption capacity of the structure was increased by about 10%. For shallow buried structure such as utility tunnels, under the premise of ensuring the structural strength of utility tunnel, higher burial depths decreased the effect of earthquake on structure, and improved its anti-seismic performance.
- The overall performance of composite precast fabricated utility tunnels with closed monolithic reinforcement was higher than that with segmented lashing reinforcement. Using this reinforcement method improved the energy dissipation capacity and bearing capacity of structures. The ductility coefficient of utility tunnel with closed monolithic reinforcement was 11.32% higher than that with segmented lashing reinforcement. However, different steel construction techniques had little effect on the stiffness of utility tunnels.
- Within a certain range, haunch height had a great effect on the anti-seismic performance of composite precast fabricated utility tunnels. After decreasing haunch height, the peak load, stiffness and energy consumption of PG5 (haunch height of 86mm) under each displacement were basically smaller than those of PG2 (haunch height of 143 mm). However, lower haunch heights were favorable for structural deformation, and the ductility coefficient of PG5 was as high as 4.93. Decreasing haunch height had a great effect on the mechanical mechanism of diagonal reinforcement at upper haunches.
- Composite precast fabricated utility tunnels showed good anti-seismic performance. The peak loads of test structure were between 315 and 379 kN, and when the bearing capacity (up to 16.6%) reached its limit value, the structures still showed high bearing capacity. The ductility coefficients of test structures were between 3.17 and 4.93, indicating their high structural deformability.

Acknowledgments

The research described in this paper was financially supported by the National Key Research and Development Plan (2017YFC0806100), Jilin Provincial Department of Education Planning Project (JJKH20190872KJ), and National Natural Science Foundation of China (51178206).

References

Abuhajar, O., El Naggar, H. and Newson, T. (2015), “Static soil culvert interaction the effect of box culvert geometric configurations and soil properties”, *Comput. Geotech.*, **69**, 219-235. https://doi.org/10.1016/j.compgeo.2015.05.005.

Chen, J., Shi, X.J. and Li, J. (2010), “Shaking table test of utility tunnel under non-uniform earthquake wave excitation”, *Soil Dyn. Earthq. Eng.*, **30**(11), 1400-1416. https://doi.org/10.1016/j.soildyn.2010.06.014.

China General Institute of Nonferrous Engineering Design and Research (2003), *Handbook for Construction of Concrete Structures*, China Architecture & Building Press, Beijing, China. (in Chinese)

Debiasi, E., Gajo, A. and Zonta, D. (2013), "On the seismic response of shallow-buried rectangular structures", *Tunnel. Underg. Space Technol.*, **38**, 99-113. https://doi.org/10.1016/j.tust.2013.04.011.

Ertugrul, O.L. (2016), "Numerical modeling of the seismic racking behavior of box culverts in dry cohesionless soils", *KSCE J. Civil Eng.*, **20**(5), 1737-1746. https://doi.org/10.1007/s12205-015-0235-1.

Huang, H.X., Li, J., Rong, X.L., Fan, P.X. and Feng, S.F. (2016), "Dynamic response of underground box structure subjected to explosion seismic wave", *Earthq. Struct.*, **10**(3), 669-680. https://doi.org/10.12989/eas.2016.10.3.669.

Jiang, L.Z., Chen, J. and Li, J. (2010), "Seismic response of underground utility tunnels: shaking table testing and fem analysis", *Earthq. Eng. Eng. Vib.*, **9**(4), 555-567. https://doi.org/10.1007/s11803-010-0037-x.

Kong, L.J. (2014), "Quasi-static test and numerical analysis of large reinforced concrete box culvert structure", Master Dissertation, Xi'an University of Architecture and Technology, Xi'an. (in Chinese)

Ma, C., Lu, D.C., Du, X.L. and Qi, C.Z. (2018), "Effect of buried depth on seismic response of rectangular underground structures considering the influence of ground loss", *Soil Dyn. Earthq. Eng.*, **106**, 278-297. https://doi.org/10.1016/j.soildyn.2017.12.021.

Ma, C., Lu, D.C., Du, X.L., Qi, C.Z. and Zhang, X.Y. (2019), "Structural components functionalities and failure mechanism of rectangular underground structures during earthquakes", *Soil Dyn. Earthq. Eng.*, **119**, 265-280. https://doi.org/10.1016/j.soildyn.2019.01.017.

Matsui, J., Ohtomo, K. and Kanaya, K. (2004), "Development and validation of nonlinear dynamic analysis in seismic performance verification of underground rc structures", *J. Adv. Concrete Technol.*, **2**(1), 25-35. https://doi.org/10.3151/jact.2.25.

Nguyen, D., Park, D., Shamsher, S., Nguyen, V. and Lee, T. (2019), "Seismic vulnerability assessment of rectangular cut-and-cover subway tunnels", *Tunnel. Underg. Space Technol.*, **86**, 247-261. https://doi.org/10.1016/j.tust.2019.01.021.

Nishioka, T. and Unjoh, S. (2003), "A simplified evaluation method for the seismic performance of underground common utility boxes", *Proceedings of the 2003 Pacific Conference on Earthquake Engineering*, Christchurch, New Zealand, February.

Park, D., Lee, T.H., Nguyen, D.D. and Park, J. (2016), "Collapse mechanism of cut-and-cover tunnels under seismic loading", *JPN Geotech. Soc. Spec. Publ.*, **2**(25), 934-937. https://doi.org/10.3208/jgssp.KOR-35.

Tsinidis, G. (2017), "Response characteristics of rectangular tunnels in soft soil subjected to transversal ground shaking", *Tunnel. Underg. Space Technol.*, **62**, 1-22. https://doi.org/10.1016/j.tust.2016.11.003.

Ulgen, D., Saglam, S. and Ozkan, M.Y. (2015), "Dynamic response of a flexible rectangular underground structure in sand: centrifuge modeling", *Bull. Earthq. Eng.*, **13**(9), 2547-2566. https://doi.org/10.1007/s10518-015-9736-z.

Xu, Z.G., Du, X.L., Xu, C.S., Hao, H., Bi, K.M. and Jiang, J.W. (2019), "Numerical research on seismic response characteristics of shallow buried rectangular underground structure", *Soil Dyn. Earthq. Eng.*, **116**, 242-252. https://doi.org/10.1016/j.soildyn.2018.10.030.

Zou, Y., Liu, H.B., Jing, L.P. and Cui, J. (2017), "A pseudo-static method for seismic responses of underground frame structures subjected to increasing excitations", *Tunnel. Underg. Space Technol.*, **65**, 106-120. https://doi.org/10.1016/j.tust.2017.02.006.

AT